

Correlation of RF impedance with Ar plasma parameters in semiconductor etch equipment using inductively coupled plasma

Cite as: AIP Advances 11, 025027 (2021); doi: 10.1063/6.0000883

Submitted: 22 December 2020 • Accepted: 28 January 2021 •

Published Online: 12 February 2021



View Online



Export Citation



CrossMark

Nayeon Lee,^{1,2} Ohyung Kwon,^{1,a)}  and Chin-Wook Chung² 

AFFILIATIONS

¹Functional Materials and Components R&D Group, Gangwon Division, Korea Institute of Industrial Technology (KITECH), Gwahakdanji-ro 137-41, Gangneung-si, Gangwon-do 25440, South Korea

²Department of Electrical Engineering, Hanyang University, 222 Wangsimri-ro, Seoul 04763, South Korea

^{a)}Author to whom correspondence should be addressed: kwonoh2000@gmail.com

ABSTRACT

The correlation of RF impedance with Ar plasma parameters was analyzed in semiconductor etch equipment using inductively coupled plasma. Since the impedance measured by a VI probe installed behind the RF bias matcher had information for plasma and structural parts of chamber simultaneously, the impedance was corrected by excluding transmission line and peripheral parts of the bias substrate. The corrected impedance was compared with plasma parameters, such as plasma density and electron temperature. The coefficient of determination between the corrected plasma resistance and the theoretical formula of the resistance for bulk plasma was over 0.9 unlike the resistance measured by the VI probe. It is expected that the corrected RF impedance can assist in monitoring the status of plasma and maintaining the quality of the etch process in semiconductor mass production lines.

© 2021 Author(s). All article content, except where otherwise noted, is licensed under a Creative Commons Attribution (CC BY) license (<http://creativecommons.org/licenses/by/4.0/>). <https://doi.org/10.1063/6.0000883>

I. INTRODUCTION

The difficulty of the plasma etch process in the semiconductor industry has gradually increased because the structures of semiconductor chips have become more complicated. Process engineers have tried to find a completely optimized plasma etching recipe for the complicated structures based on the experience obtained in trial and error and the knowledge of the basic chemistry and physics of the plasma process.¹ Basic plasma parameters, such as electron density, electron temperature, and DC bias voltage, are useful to understand the plasma etch process and to determine the proper recipe. However, it is impossible to directly measure the plasma parameters during the plasma etch process by using an invasive plasma monitoring method because inserting a probe into an industrial process chamber is disallowed. The VI probe is one of the appropriate methods to non-invasively monitor the status of plasma because the VI probe can be installed at the outside of the process chamber. The VI probe can measure the voltage, current, and phase difference of RF

power, which can be located in front of or behind a RF matcher. Voltage is measured by a high-voltage probe or a metal plate for capacitive coupling, and current is measured by a coil for inductive coupling. Phase difference is calculated by real and imaginary parts of voltage and current. The VI probe can be used to infer plasma impedance,² which consists of plasma resistance, plasma inductance, and sheath capacitance because a plasma can be considered as an electric component.

There have been many studies about measuring electrical characteristics, such as voltage, current, and impedance to monitor the status of plasma. Butterbaugh *et al.*³ studied minimizing a stray impedance by using a tri-axial power feedthrough and an electrode shield configuration for accurate measurements of plasma impedances. Spiliopoulos *et al.*⁴ measured plasma impedances in a parallel-plate CVD reactor by inserting a stray resistance. Patrick *et al.*⁵ obtained plasma impedances by controlling capacitor positions of a matching network attached to a transformer coupled plasma source. Roth *et al.*⁶ measured plasma impedances to

analyze the characteristics of the plasma etch process. Yang *et al.*⁷ proposed that a wafer voltage was derived from RF measurements from the bias electrode based on the transmission line properties of a bias input port, and the wafer voltage was used to control a DC wafer clamping voltage. Bora *et al.*⁸ used electrical discharge characteristics to evaluate the plasma parameters of capacitive-coupled Ar plasma based on the modified homogeneous discharge model. Tanisli *et al.*⁹ investigated the electrical properties of bulk plasma and sheath capacitance at low pressure using a homogeneous discharge model of capacitive-coupled RF plasma. Park and Chung¹⁰ proposed a non-invasive plasma monitoring method that used a RF substrate without the insertion of a probe. However, there have been no studies about correlations between RF impedances and plasma parameters in a plasma etch chamber for mass production. Furthermore, although electrical characteristics acquired by the VI probe located behind a RF matcher necessarily contained the impedances of fixed structural chamber parts, none of the previous studies have excluded the chamber parts to correct the RF impedance measured by the VI probe. Considering a transmission line of the chamber and peripheral parts of electrostatic chuck (ESC), a plasma chamber circuit model was proposed, and then, the impedance of plasma was extracted. Finally, the impedance of plasma was compared with the plasma parameters measured by the floating harmonic method.¹¹

The present work is organized as follows. In “Sec. II,” experimental settings and chamber circuit models are given. In “Sec. III,” as source power, bias power, and process pressure were varied, correlations of the corrected RF impedances with Ar plasma parameters are presented. The final section is a conclusion.

II. EXPERIMENTAL SETUP AND METHODOLOGY

A. Experimental settings

Experiments were carried out in the semiconductor mass-production etch equipment known as “conductor etcher” or “poly etcher.” The equipment had two RF power sources, which were supplied to a planar-type RF coil (source power) and an ESC through a transmission line (bias power), respectively. Figure 1 shows a schematic diagram of the equipment. The quartz window separated the coil and a process chamber. The vertical distance between the quartz window and the ESC was over 150 mm. A 300 mm wafer was positioned on the ESC of Johnsen–Rahbek type. There were several ceramic parts on the periphery of ESC to shield the ESC against harsh plasma circumstances and to block a breakdown between the ESC and metal ground. The inside of ESC was composed of a metal body having a coolant flow path and a ceramic puck containing a chucking electrode and a heating electrode. All frequencies of two RF power sources were 13.56 MHz, and the phases were synchronized. Ar was used as the process gas in this study, and the flow rate of Ar was fixed at 200 SCCM. The temperatures of the ESC and chamber wall were set at 25 °C and 60 °C, respectively.

The VI probe (Rainbow Corporation, South Korea) used in this study was located behind a bias RF matcher or in front of a RF rod (transmission line). The total length of the transmission line was 720 mm of which the shape was coaxial type. The VI probe

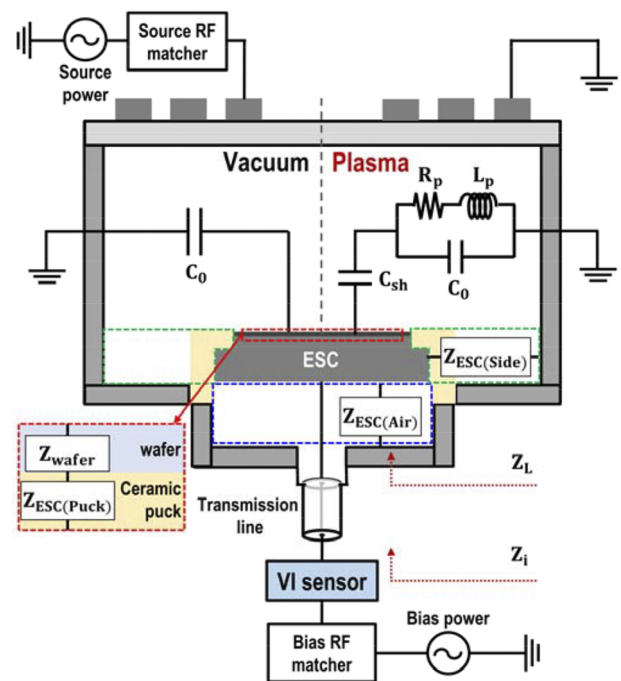


FIG. 1. Schematic diagram of the semiconductor etch equipment used in this study.

consisted of a voltage sensor using a metal plate and a current sensor using a coil in one body, and it was combined with the inner metal rod of the transmission line. The analog signals were captured by an oscilloscope (DPO-3024, Tektronix, United States) and processed by LabVIEW in real time. The sampling rate of the oscilloscope was set at 2.5 GHz. PCI extensions for the instrumentation controller (PXIe-8840, NI, United States) had a 2.6 GHz quad-core processor and 4 GB memory. The amplitude and phase difference of RF voltage and RF current were collected by signal processing to separate the real and imaginary parts.¹² The floating harmonic method (WISE probe, P&A solutions, South Korea) was used to measure plasma parameters, such as ion density and electron temperature. A probe tip was positioned at 20 mm above a wafer. Before measuring the plasma parameters, the chamber was run for 1 h for accurate measurements.

B. Plasma chamber circuit modeling

Since the VI probe necessarily measured electrical characteristics including all impedances of equipment parts, which were exposed to or hidden from plasma, the impedances of equipment parts had to be excluded to obtain a little more genuine plasma. Before building a plasma circuit model, first, a circuit diagram was designed based on the placement of equipment parts when the chamber contained a vacuum, and then, the impedance of the chamber was measured by using a network analyzer. The network analyzer was connected to the almost same location as the VI probe with a proper zig. When a part could be brought out from the

chamber, the impedance of the eliminated part was determined by the change of the impedance. On the other hand, when a part could not be removed in the chamber, the impedance was calculated by general formulas for electronic components. Figure 2(a) shows a circuit diagram when the chamber contained a vacuum. The proposed circuit diagram consisted of a vacuum space, ESC ceramic puck, wafer, peripheral parts of ESC, and a transmission line. The circuit diagram was focused on only bias power supply path because the impedance measured by a network analyzer was constant whether the chamber lid including the quartz window and RF coil was covered or uncovered.

The transmission line in the chamber was coaxial type, and the role was to supply a bias power to the ESC. The impedance measured by a network analyzer or VI probe (Z_i) was changed to Z_L after passing through the transmission line as follows:

$$Z_L = Z_0 \frac{Z_i - Z_0 \tanh(\gamma l)}{Z_0 - Z_i \tanh(\gamma l)}, \tag{1}$$

$$Z_0 = \sqrt{\frac{R + j\omega L}{G + j\omega C}}, \tag{2}$$

$$\gamma = \sqrt{(R + j\omega L)(G + j\omega C)}. \tag{3}$$

Here, Z_0 is the characteristic impedance of the line, γ is the propagation constant of the line, l is the length of the transmission line, and ω is the RF frequency. The transmission line in the chamber was composed of ten parts, which had different dimensions and distributed parameters (R , L , G , and C). These parameters for a

coaxial transmission line were derived by calculating simple electrical formulas.¹³ The real part (R_0) of Z_i measured by the network analyzer was considered as a parasitic resistance, which came from joints of metal parts, and it was added in the circuit diagram in series. The imaginary part of Z_i was a negative value, and the imaginary part of Z_L became a more negative value because passing through the line meant to closely approach toward the load impedance.

Peripheral parts of the ESC were considered as capacitances because these were between the ESC and ground. The first peripheral part was the capacitor with an air gap below the ESC ($Z_{ESC(Air)}$), and the second peripheral part was the capacitor with a ceramic structural part and air gap beside the ESC ($Z_{ESC(side)}$). $Z_{ESC(Air)}$ was calculated by using the formula for the capacitance of a parallel plate capacitor. $Z_{ESC(side)}$ was derived by the aforementioned method eliminating the part and measuring the change of impedance. The impedance of a ceramic puck of the ESC and wafer ($Z_{ESC(puck)}$ and Z_{wafer}) was also calculated by the formula for the capacitance of a parallel plate capacitor. The dielectric constants of the ceramic puck and wafer were 10 and 11.4, respectively. The resistivity of the ceramic puck and wafer was neglected. Finally, after all impedances of parts were determined, the impedance of a vacuum space (C_0) could be simply calculated from Z_i , which was a capacitance between a wafer and metal wall ground. Table I shows Z_i and Z_L measured by a network analyzer when the chamber contained a vacuum, and the impedances of peripheral parts of the ESC and vacuum space.

When there was a plasma in the chamber, a homogeneous model of capacitively coupled plasma² was used as a plasma circuit in this study. Figure 2(b) shows a circuit diagram when a plasma was on. The impedance including sheath capacitance (C_{sh}), plasma

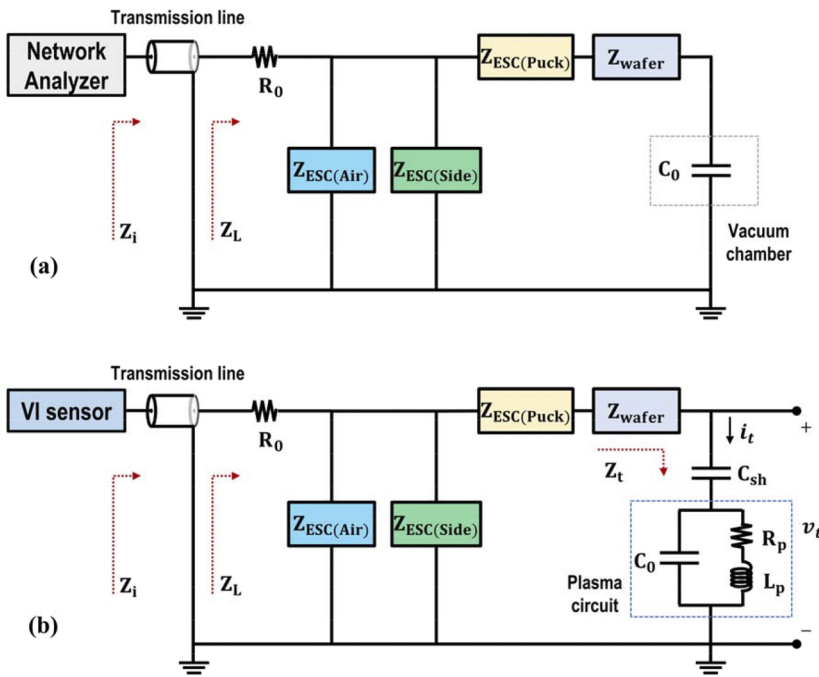


FIG. 2. Circuit diagrams (a) when the chamber contained a vacuum and (b) when plasma was on.

TABLE I. The impedances to build circuit diagrams when the chamber contained a vacuum or there was a plasma in the chamber at the condition of a source power of 400 W, bias power of 100 W, and 5 mTorr.

State of chamber	Z_i (Ω)	Z_L (Ω)	$Z_{ESC(Air)}$ (k Ω)	$Z_{ESC(Side)}$ (Ω)	$Z_{ESC(Puck)}$ (Ω)	Z_{wafer} (Ω)	C_0 (pF)	Z_t (Ω)	C_{sh} (pF)	R_p (Ω)	L_p (nH)
Vacuum	0.3 – 15.9j	0.3 – 36.0j	–4.49j	–143j	–1.94j	–1.23j	258
Plasma	2.41 – 7.45j	2.47 – 14.3j						2.69 – 12.8j	919	2.68	1.86

resistance (R_p), plasma inductance (L_p), and C_0 referred to Z_t , which was separated into the impedance of a sheath and a plasma circuit. As can be seen in Fig. 3, since the phase of Z_t was close to -80° , the imaginary part of Z_t (X_t) was capacitive and the amplitude of Z_t was almost the same as the amplitude of X_t . Therefore, it was assumed that X_t was the capacitance of sheath and the RF voltage applied across Z_t was mostly applied across the sheath. The sheath capacitance was obtained as follows:

$$X_t \approx \frac{1}{j\omega C_{sh}}, \tag{4}$$

$$C_{sh} \approx \frac{|i_t|}{\omega |v_t|}, \tag{5}$$

where i_t is the current flowing through the plasma circuit and v_t is the voltage applied across the plasma circuit. According to the above assumption, the real part of Z_t (R_t) is the impedance of the parallel circuit of ($R_p + j\omega L_p$) and C_0 as follows:

$$R_t = (R_p + j\omega L_p) \parallel \left(\frac{1}{j\omega C_0} \right), \tag{6}$$

$$R_p = \frac{R_t}{1 + \omega^2 R_t^2 C_0^2}, \tag{7}$$

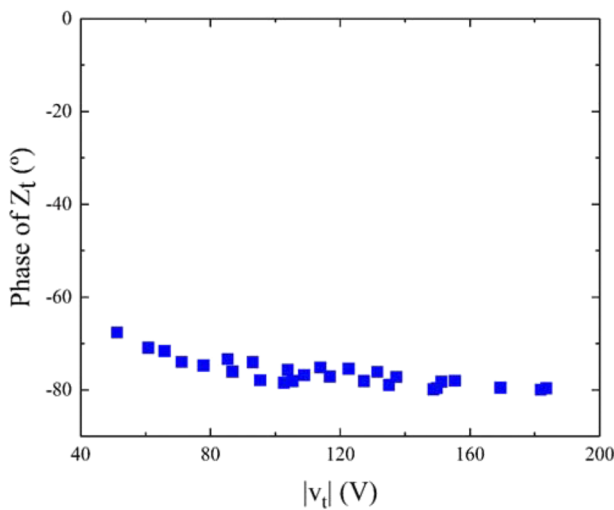


FIG. 3. Phase of Z_t with the amplitude of the voltage applied across Z_t .

$$L_p = \frac{R_t^2 C_0}{1 + \omega^2 R_t^2 C_0^2}. \tag{8}$$

By using Eqs. (7) and (8), we could obtain R_p and L_p because R_t and C_0 were already known. Table I also shows an example of Z_i , Z_L , Z_t , C_{sh} , R_p , and L_p when there was a plasma in the chamber at the condition of a source power of 400 W, bias power of 100 W, and 5 mTorr. Using the above-mentioned procedure, the corrected RF impedances could be drawn from the Z_i value measured by the VI probe and were analyzed whether it was close to plasma parameters in “Sec. III.”

III. RESULTS AND DISCUSSION

Plasma density (N_i) and electron temperature (T_e) were changed by varying source power, bias power, and pressure as shown in Fig. 4. The bias power was defined as the measured power by the VI probe same as the power supplied from the RF bias generator minus the power consumed by the RF bias matcher because the bias matcher consumed the power nonlinearly as the supplied power increased. The source power was defined as the power supplied from the RF source generator. The plasma density was increased with the increase of source power or pressure, but the bias power had no effect on changing the plasma density. The electron temperature was decreased with the increase of pressure, but different trends were shown for other variables. When the bias power was 200 W over, the electron temperature was slightly decreased or saturated with the increase of the source power, whereas when the bias power was 100 W, the electron temperature of 10 mTorr below was slightly increased and that of 15 mTorr was decreased with the increase of the source power. However, electron temperatures of the same pressure were averagely similar regardless of the source power or bias power.

Real (R_i) and imaginary (X_i) parts of Z_i measured by the VI probe were investigated and are shown in Fig. 5. When the bias power increased, R_i was also roughly increased at the same condition of pressure or source power, whereas R_i was irregularly changed with respect to the source power. The irregular tendency of R_i made it ambiguous to analyze a relation between the impedance measured by the VI probe and plasma parameters. This was the reason why the corrected RF impedance was needed to monitor the status of plasma when using the VI probe. On the other hand, X_i was increased with the increase of the source power or pressure and was decreased with the increase of the bias power. The trend of X_i was similar to plasma density for all process variables except for bias power, and it could

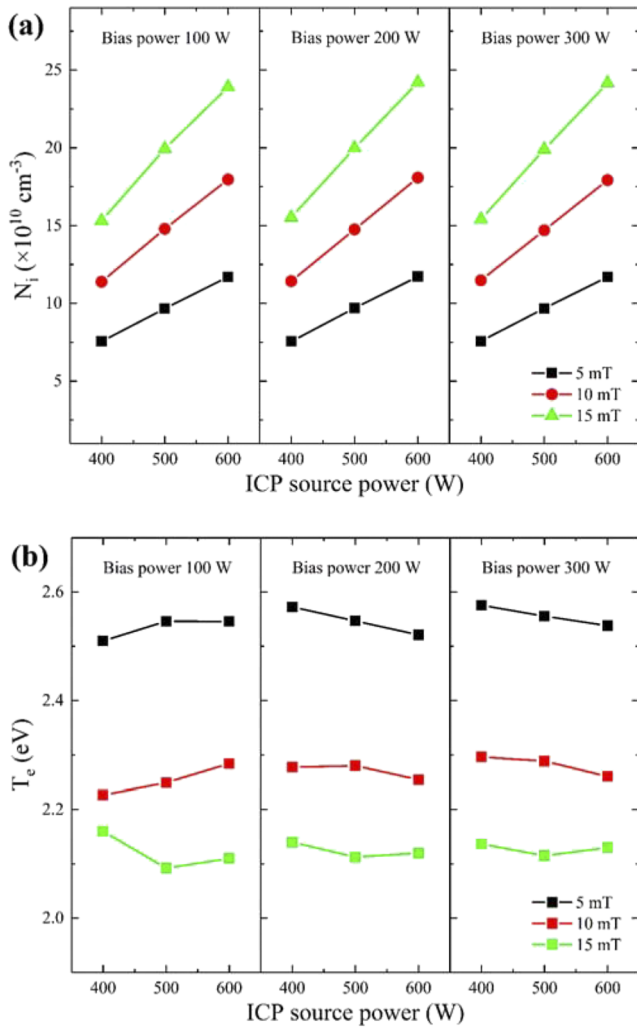


FIG. 4. (a) Plasma density and (b) electron temperature with the varying source power, bias power, and pressure.

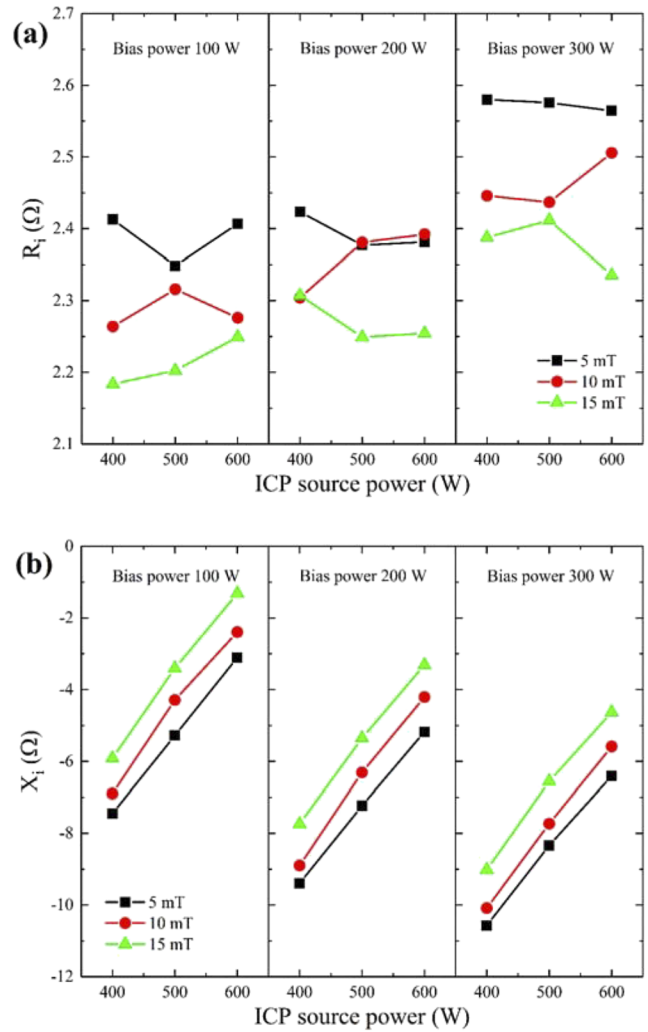


FIG. 5. (a) Real part (R_i) and (b) imaginary part (X_i) of the impedance measured by the VI probe with the varying source power, bias power, and pressure.

be considered that X_i had information about both bulk plasma and sheath.

As opposed to R_i , R_p showed a regular tendency for all process conditions as shown in Fig. 6. R_p was decreased with the increase of the source power or pressure and increased with the increase of the bias power. L_p was similar to R_p . C_{sh} was increased nonlinearly with the increase of the source power. Although R_p and L_p were changed by the bias power, the regular tendency of R_p and L_p was useful for analyzing the relation between the RF impedance and plasma parameters. The amplitudes of v_t and i_t were also investigated and are shown in Fig. 7. The amplitude of v_t was increased with the increase of the bias power and decreased with the increase of the source power or pressure. The amplitude of i_t was increased with the increase of the source power, bias power, and pressure, but the change of i_t for the source power

and pressure was relatively small because the VI probe measured the impedance of capacitively coupled plasma driven by the RF voltage.

The resistance of bulk plasma was theoretically proportional to $\sqrt{T_e}/N_i$ when considering the Ohmic heating and hard wall model for stochastic heating in low-pressure capacitive RF discharges.^{8,14} Since the information about bulk plasma and sheath in R_p was combined, the relation between resistances and plasma parameters was separately analyzed for each bias power. Figure 8 shows the coefficient of determination (R-squared) between $\sqrt{T_e}/N_i$ and R_i or R_p . The corrected plasma resistance R_p had a higher R-squared than R_i , and it could be considered that R_p represents the bulk plasma unlike R_i . The R-squared between N_i and C_{sh} was also investigated and is shown in Fig. 9. Contrary to the case of R_p , the R-squared values were about 0.68 even at the same condition of bias power. It was

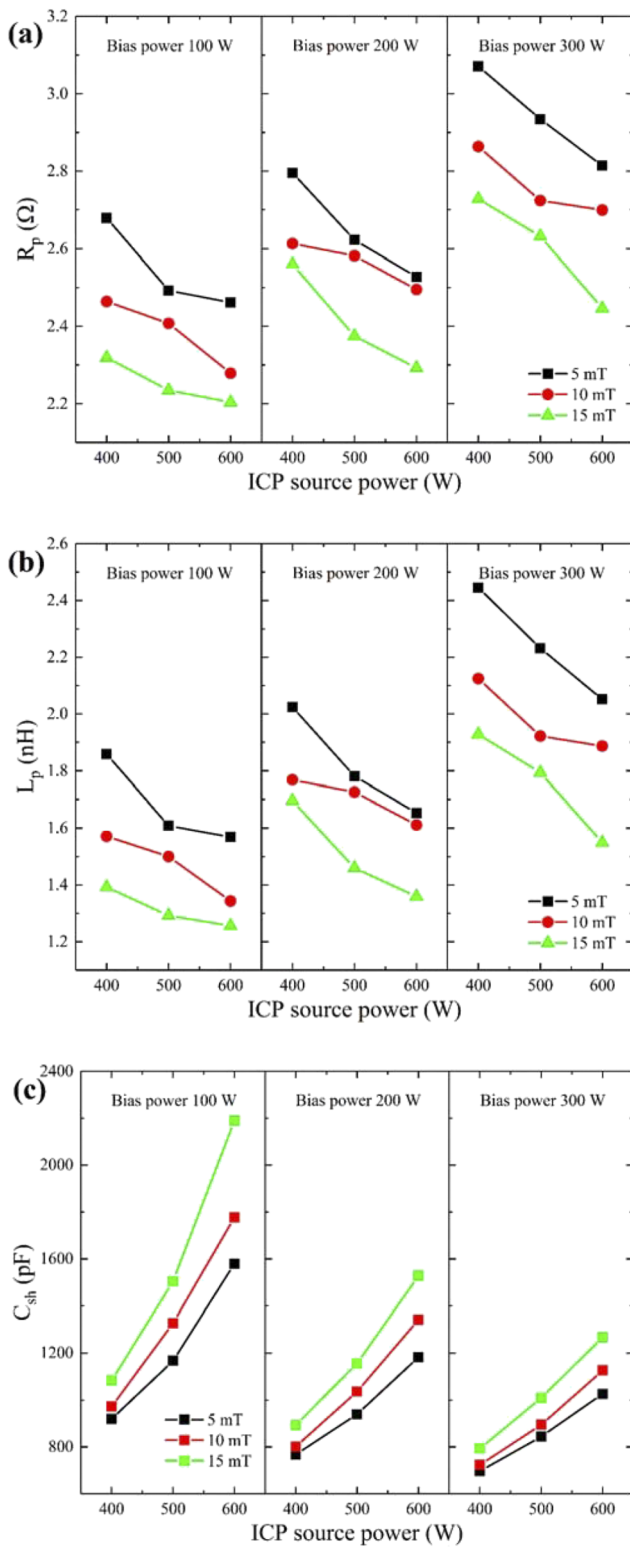


FIG. 6. (a) Plasma resistance (R_p), (b) plasma inductance (L_p), and (c) sheath capacitance with the varying source power, bias power, and pressure.

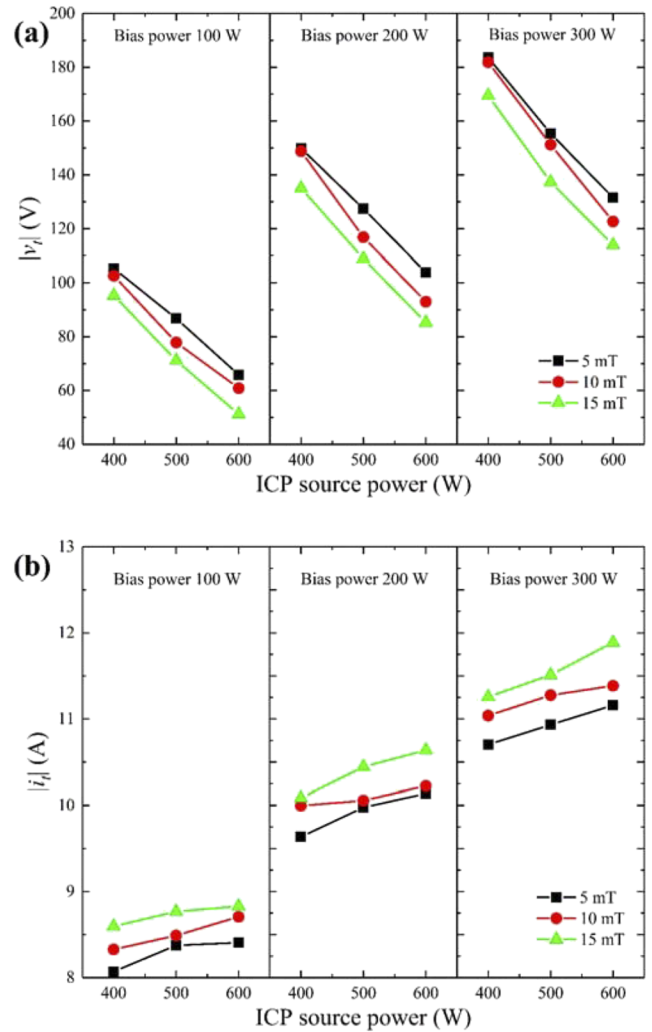


FIG. 7. Amplitude of (a) the voltage applied across Z_i and (b) the current flowing through Z_i with the varying source power, bias power, and pressure.

presumed that C_{sh} is related to another plasma parameter as well as bulk plasma.

The electron-neutral collision frequency could also be derived by using the corrected RF impedance, and it was compared with that derived by using plasma parameters. According to a homogeneous model of capacitively coupled plasma,² R_p and L_p can be expressed as follows:

$$R_p = \nu_{en} L_p, \quad (9)$$

where ν_{en} is the electron-neutral collision frequency, which is R_p over L_p . The electron-neutral collision frequency derived by using plasma parameters is expressed as follows:¹⁵

$$\nu_{en} \approx 2.3 \times 10^6 \cdot p \cdot \sqrt{T_e}, \quad (10)$$

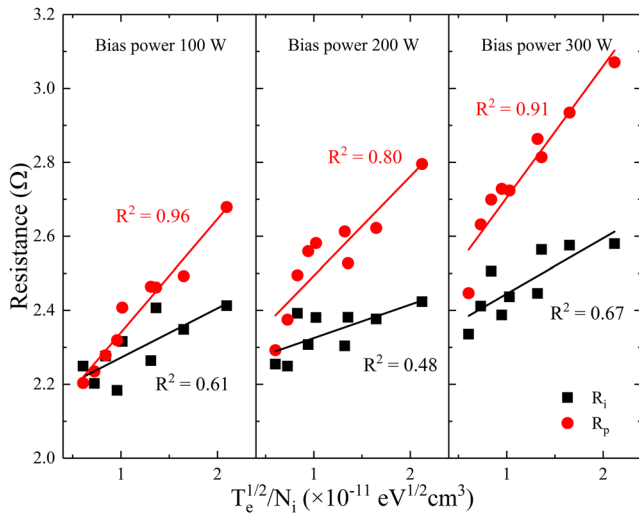


FIG. 8. Coefficient of determination (R-squared) between $\sqrt{T_e}/N_i$ and R_i or R_p for each bias power.

where p is the pressure (mTorr). Figure 10 shows the electron-neutral collision frequencies obtained by two methods. The values obtained by the two methods differed by about two orders of magnitude, and therefore, R_p and L_p were hard to be used in quantitative research. However, the values from both of the methods were increased with the increase of pressure as similar as a previous study.¹⁶ As stated above, the corrected impedance was matched with plasma parameters qualitatively, and it is expected that using the corrected impedance is useful for indirectly monitoring the status of plasma in real time.

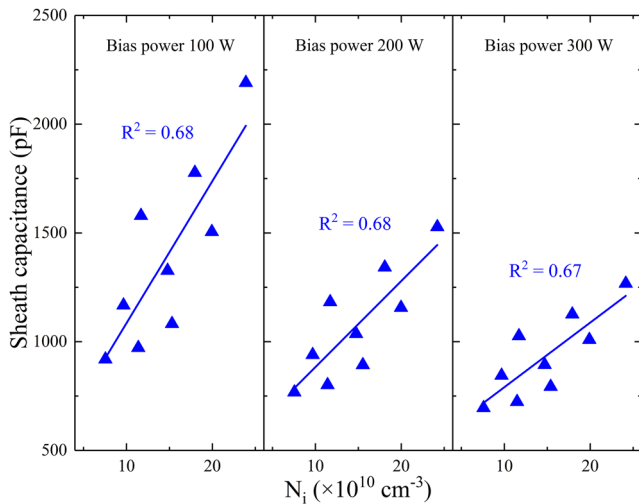


FIG. 9. Coefficient of determination (R-squared) between N_i and C_{sh} for each bias power.

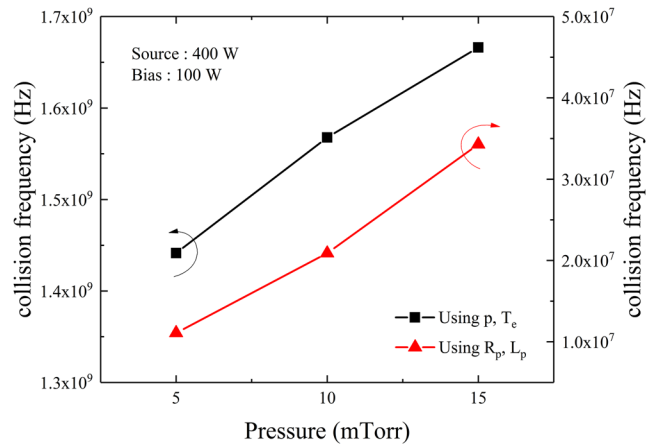


FIG. 10. Electron-neutral collision frequencies obtained by using plasma parameters (pressure and electron temperature) and using plasma resistance and plasma inductance.

IV. CONCLUSIONS

We investigated the correlation of RF impedance with Ar plasma parameters in a plasma etch chamber. First of all, the impedance measured by the VI probe installed behind the RF bias matcher was corrected by excluding transmission line and peripheral parts, and the corrected impedance was compared with plasma parameters, such as plasma density and electron temperature. Plasma resistance and plasma inductance were validated by comparing with theoretical formulas. The R-squared between the corrected plasma resistance and the formula for the resistance of bulk plasma was over 0.9, and the electron-neutral collision frequency derived by the corrected impedance had a similar tendency to that derived by plasma parameters. Since plasma parameters in this study were measured at bulk plasma, the analysis for sheath capacitance was insufficient and expects to be progressed afterward. Nevertheless, the corrected impedance can be used for indirectly monitoring the status of plasma in mass-production equipment without invasion into the chamber and assist in maintaining the quality of the etch process.

ACKNOWLEDGMENTS

This work was supported by the National Research Foundation of Korea (NRF) grant funded by the Korea government [Ministry of Science and ICT (MSIT)] (Grant No. 2019R1C1C1010062).

DATA AVAILABILITY

The data that support the findings of this study are available within the article.

REFERENCES

- ¹K. J. Kanarik, *J. Vac. Sci. Technol.*, **A 38**(3), 031004 (2020).
- ²M. A. Lieberman and A. J. Lichtenberg, *Principles of Plasma Discharges and Materials Processing* (John Wiley & Sons, Inc., New York, 1994).

- ³J. W. Butterbaugh, L. D. Baston, and H. H. Sawin, *J. Vac. Sci. Technol., A* **8**(2), 916–923 (1990).
- ⁴N. Spiliopoulos, D. Mataras, and D. E. Rapakoulas, *J. Vac. Sci. Technol., A* **14**(5), 2757–2765 (1996).
- ⁵R. Patrick, C.-G. Lee, S. E. Hilliker, and R. D. Moeller, *J. Vac. Sci. Technol., A* **15**(3), 1250–1256 (1997).
- ⁶W. C. Roth, R. N. Carlile, and J. F. O'Hanlon, *J. Vac. Sci. Technol., A* **15**(6), 2930–2937 (1997).
- ⁷J. G. Yang, D. J. Hoffman, S. C. Shannon, D. H. Burns, W. Lee, and K.-S. Kim, U.S. patent 7,375,947 (20 May 2008).
- ⁸B. Bora, H. Bhuyan, M. Favre, E. Wyndham, H. Chuaqui, and C. S. Wong, *Curr. Appl. Phys.* **13**, 1448–1453 (2013).
- ⁹M. Tanisli, N. Sahin, and S. Demir, *Pramana* **89**, 36 (2017).
- ¹⁰J.-H. Park and C.-W. Chung, *J. Vac. Sci. Technol., A* **36**(3), 031302 (2018).
- ¹¹M.-H. Lee, S.-H. Jang, and C.-W. Chung, *J. Appl. Phys.* **101**, 033305 (2007).
- ¹²K.-H. Jang, S.-Y. Park, J.-J. Choi, and D.-H. Lee, *J. Korean Inst. Electromagn. Eng. Sci.* **29**(7), 484–490 (2018).
- ¹³D. K. Cheng, *Field and Wave Electromagnetics* (Addison-Wesley, 1989).
- ¹⁴T. Mussenbrock, R. P. Brinkmann, M. A. Lieberman, A. J. Lichtenberg, and E. Kawamura, *Phys. Rev. Lett.* **101**, 085004 (2008).
- ¹⁵Y. P. Raizer, M. N. Shneider, and N. A. Yatsenko, *Radio-Frequency Capacitive Discharges* (CRC Press LLC, 1995).
- ¹⁶K. H. You, S. J. You, D. W. Kim, B. K. Na, B. H. Seo, J. H. Kim, and H. Y. Chang, *Phys. Plasmas* **23**, 033509 (2016).